Cross-Field Electron Thermal Conductivity in an Electron-Beam–Plasma System

D. D. Needelman and R. L. Stenzel
Department of Physics, University of California, Los Angeles, Los Angeles, California 90024
(Received 11 June 1986)

The cross-field electron thermal conductivity coefficient, $\kappa_\perp$, in an electron-beam–heated cylindrical magnetoplasma ($n_0 \sim 3\times10^{11}$ cm^{-3}; $|\mathbf{B}_0| = 30$ G, 120 G; $V_b = 200$ V; $I_b \le 2.5$ A, $t_b \le 5$ μs) is measured. Results are compared with classically predicted values. After beam turnoff, $\kappa_\perp$ approaches within a factor of 3 the classical value, except for the case $I_b = 1.5$ A, $|\mathbf{B}_0| = 120$ G. For that case, and during the beam pulses, $\kappa_\perp$ is found to be anomalously high, by up to over 2 orders of magnitude above the classical value.

PACS numbers: 52.25.Kn, 52.25.Fi

Heat-transport studies in a plasma are important in fusion engineering and space physics, among other fields. Electron heat flow across a magnetic field, due to an electron thermal gradient, was theoretically analyzed,[1] then experimentally verified,[2] for the case of not very strong fields, i.e., $\omega_{ce}/\nu_e \sim 6$ (ω_{ce} is the electron cyclotron frequency; ν_e is the electron collision frequency). Analysis of such heat flow for strong fields ($\omega_c \gg \nu_e$) yields the transport coefficients used in this paper.[3]

In the experiment, cross-field heat transport is observed from the electron-beam–heated central axis (the "beam flux tube," radius $r \le 1.27$ cm) of a cylindrical plasma, to $r = 3.4$ cm off axis. The beam produces turbulent Langmuir waves of various phase velocities. Some of these trap background electrons, producing energetic electron tails ($\sim$10–50 eV) as they damp, to heat the background.[4] Negatively biased grids, placed 1 and $\sim$35 cm from the beam cathode face, axially confine the heat of the background electrons to a limited region, leaving radial heat diffusion as the major loss mechanism. The cross-field electron thermal-conductivity coefficient is then obtained from probe measurements of $kT_e(r,t)$ and $n_e(r,t)$.

Theory predicts that for a simple two-component (electrons and singly charged ions) magnetoplasma, the total electron heat flux, $\mathbf{q}^e$, may be represented as the sum of frictional heat flux, $\mathbf{q}^e_u$, and thermal-gradient heat flux, $\mathbf{q}^e_T$. The former diffuses heat among the electrons through unlike-particle collisions, assuming a nonzero relative streaming velocity, $\mathbf{u}$. For the cases considered here, $\mathbf{q}^e$ is

$$\mathbf{q}^e = 0.71 nkT_e u_\parallel + \frac{3}{2}\frac{nkT_e}{\omega_{ce}\tau_e}\hat{\mathbf{b}}\times(\mathbf{u}_\phi + \mathbf{u}_r) - \kappa_\parallel \nabla_\parallel (kT_e) - \kappa_\perp \nabla_\perp (kT_e) - \kappa_\Lambda \hat{\mathbf{b}}\times\nabla_\perp (kT_e), \tag{1}$$

where the field is $\mathbf{B}_0 = B_0\hat{\mathbf{b}}$; τ_e is the electron/ion collision time; and $\kappa_\parallel$, κ_Λ, and $\kappa_\perp$ are the electron thermal conductivity coefficients.

The particle-conservation and energy-transport equations for the electron species are

$$\frac{\partial n}{\partial t} + \nabla\cdot(n\mathbf{v}_e) = S, \tag{2}$$

$$\tfrac{3}{2}SkT_e + \tfrac{3}{2}n\left[\frac{\partial (kT_e)}{\partial t} + \mathbf{v}_e\cdot\nabla(kT_e)\right] + nkT_e\nabla\cdot\mathbf{v}_e = -\nabla\cdot\mathbf{q}^e - \mathbf{P}:\nabla\mathbf{v}_e + Q, \tag{3}$$

where $n_e = n_i = n$, S is the source for electrons, $\mathbf{P}$ is the electron stress tensor, and Q is the electron heat source.

The experimental design allows the following simplifications: $\mathbf{u}_\phi$ is caused by the $\nabla_p\times\mathbf{B}$ electron drift (as confirmed by comparison of measurements made in both 30- and 120-G fields); $\mathbf{u}_\parallel \sim \mathbf{0}$, as background electrons, reflected by the grids, do not exhibit axial drifts; elastic collisions of electrons with ions and neutrals do not act as an electron heat source/sink on the 45-μs time scale of this experiment; $\nabla\cdot[\kappa_\Lambda\hat{\mathbf{b}}\times\nabla_\perp(kT_e)]$ is 0, as azimuthal heat flow carries heat only along isotherms; axial uniformity is maintained between the grids ($\nabla_\parallel \sim 0$) through rapid axial transport up to the confining grids (measurements made along the central axis of the system during and after a 200-V, 1.5-A beam pulse indicate that $|\nabla_\parallel kT_e/kT_e| \sim |\nabla_\parallel n/n| < 0.02$/cm); and azimuthal symmetry is maintained. The last two conditions result in time and the radial position being the only independent coordinates.

From the stress-tensor component equations,[5] $\mathbf{P}:\nabla\mathbf{v}$ may be evaluated as $-0.24nkT_e\tau_e(\partial v_r/\partial_r + v_r/r)^2$ ($v_r = \mathbf{v}_e\cdot\hat{\mathbf{r}}$, $\partial/\partial\phi = \partial/\partial z = 0$).

From the above, $\kappa_\perp$ may be calculated to be

$$\kappa_{\perp\,\text{measured}}(r,t) = \int_0^r r'\left\{\tfrac{3}{2}n\left[\frac{\partial}{\partial t}(kT_e) + v_r\frac{\partial}{\partial r'}(kT_e)\right] + kT_e\left[\tfrac{5}{2}S - \frac{\partial n}{\partial t} - v_r\frac{\partial n}{\partial r'} - 0.24n\tau_e\left(\frac{\partial v_r}{\partial r} + \frac{v_r}{r}\right)^2\right] - Q\right\}dr' \times\left[r\frac{\partial(kT_e)}{\partial r'}\bigg|_{r'=r,t}\right]^{-1} - 1.5\left[\frac{kT_e}{m\omega_{ce}^2\tau_e}\right]\frac{\partial(nkT_e)}{\partial r}\left[\frac{\partial(kT_e)}{\partial r'}\bigg|_{r'=r,t}\right]^{-1}. \tag{4}$$

The classical cross-field electron thermal-conductivity coefficient for a two-component magnetoplasma is given by[3] $\kappa_{\perp\,\text{predicted}}(r,t)=4.7nkT_e/m\omega_{ce}^2\tau_e$.

The experimental setup is depicted in Fig. 1. A pulsed magnetized-discharge plasma column (argon pressure $=1.3\times10^{-4}$ Torr, chamber base pressure $=2.0\times10^{-6}$ Torr, axial $B_0=30$, 120 G, $|\nabla B_0/B_0|\leq0.001$/cm) is created by use of a BaO-coated cathode. The resultant afterglow plasma density and electron temperature decay exponentially in time, with respective decay times $\tau_n\sim630$ μs, $\tau_{kT_e}\sim770$ μs. (As the plasma decays through axial losses, τ_n and τ_{kT_e} are independent of $|\mathbf{B}_0|$.) The afterglow plasma is heated by an electron beam fired along the central axis by a 2.5-cm-diameter BaO-coated cathode ($V_b=200$ V, $\tau_b=3$–5 μs) applied typically at 600 μs into the afterglow ($kT_e=0.3$ eV, $n=3\times10^{11}$ cm). Heating occurs within 5 cm of beam injection. The grids used for electrostatic axial heat and particle confinement are pulsed negatively ($V_g=-150$ V, $\tau_g=45$ μs, with V_g attained 1 μs prior to beam firing), so that $V_b>-V_g\gg\max(kT_e/e)$, allowing only beam electrons to pass. (The grids partially trap the electron tail.) The grids' diameter, 10 cm, is much greater than that of the beam flux tube, preventing heat and particle leakage around the edges. kT_e and n are measured only during the grid pulse. As $\tau_g\ll\tau_n,\tau_{kT_e}$, measured changes in n and kT_e are independent of plasma decay.

Plasma parameters are measured with a single-sided pulsed Langmuir probe (area $=0.75$ mm^2) midway between the grids. Radial position is adjusted during a data run. The probe face normal is perpendicular to the beam path. This avoids interference from the energetic tail electrons along $\mathbf{B}_0$, during and shortly after the beam pulse. (The beam tail lasts ~3 μs after the beam pulse,[6] with a decay due to inelastic collisions.) Probe current is sampled ($\Delta t=100$ ns) for temporal resolution; probe current versus probe voltage is plotted over ~500 shots. The plots from various probe positions and sample times yield a temporal and spatial map of kT_e and n.

As described below, $kT_e(r,t)$ and $n(r,t)$ are used to derive the following quantities: their partial derivatives with respect to time and space; the particle source, $S(r,t)$; the electron radial velocity, $v_r(r,t)$; $\partial v_r/\partial r$; and the heat source, $Q(r,t)$. With these terms in the integrand of (4) calculated, Simpson's rule is used to compute the integral. $\kappa_\perp$ may be easily calculated from this.

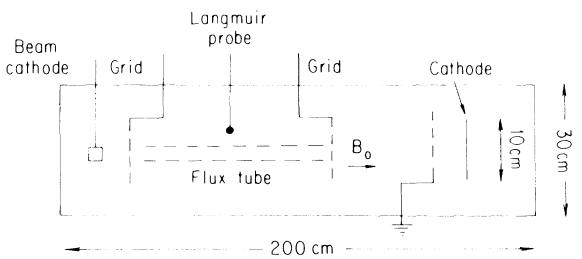

FIG. 1. Experimental setup.

Partial derivatives of kT_e are taken after the finding of suitable functions which are least-squares fitted to the measurements of kT_e. Temporally, kT_e is seen to rise and fall exponentially. For evaluation of $\partial(kT_e)/\partial t$, at position r_i, the function $kT_e(t)=A_i\exp(-B_it^{C_i})+D_i$ is fitted to the temperature measurements. As S and Q are discontinuous at beam turnoff, (2) and (3) imply discontinuities in derivatives of kT_e and n. Therefore, different choices of A_i, B_i, C_i, and D_i are indicated for the periods of temperature rise and fall. $\partial n/\partial t$ is evaluated similarly.

The cylindrical symmetry of the beam/plasma system suggests fitting of a summation of Bessel functions to measurements of kT_e in order to evaluate $\partial(kT_e)/\partial r$. Discontinuities exist in the derivatives of kT_e and n at the edge of the beam flux tube; these were found to be far less pronounced than the temporal derivative discontinuities. At any given time t_i, one function may be used to approximate $kT_e(r)$, for all r. As the function must be evaluated at $r=0$, only Bessel functions of the first kind, J_γ, may be used in the summations. Use of only J_0 and J_1 proved to give an accurate fit ($\sim\pm10\%$); i.e., the function used for time t_i is $kT_e(r)=A_i'J_0(a_ir)B_i'J_1(b_ir)+C_i'$. $\partial n/\partial r$ is evaluated similarily.

To evaluate S, the particle source/sink, $\int S\,dV$, is solved by use of the integral of (2) over the volume between the grids. (All spatial integrals in this paper are evaluated over the volume between the grids.) $\int\nabla\cdot(n\mathbf{v}_e)dV$ is taken to be 0, as particle flux through a cylindrical surface >3 cm from the beam axis is seen to be negligible. If we assume that S is nonzero, and uniform, only for a volume V_0 contained in the volume between the grids, $\int S\,dV$ reduces to SV_0. Electrons put into the system are assumed to originate from the beam-flux tube; for $\int S\,dV>0$, V_0 is taken to be the beam-flux tube volume. Electrons lost from the system are assumed to flow out radially (as the grids block axial flow); for $\int S\,dV<0$, V_0 is approximated to be the volume of the cylindrical region between the final two radial measurements. Dividing $\int S\,dV$ by the relevant V_0 gives S.

With knowledge of S, (2) is used to calculate v_r and $\partial v_r/\partial r$. With use of n, and the procedure described above to calculate $\partial n/\partial t$ and $\partial n/\partial r$, v_r and $\partial v_r/\partial r$ are solved for numerically. The Runge-Kutta method of order 4 is used, with the boundary condition $v_r(r=0,t)=0$ for all t.

Q, the energy source/sink, is calculated in the same fashion as S. $\int Q\,dV$ is evaluated by use of the integral of (3). $\int\nabla\cdot\mathbf{q}_T^e\,dV$ is taken to be 0, as the thermal-gradient heat flux through a cylindrical surface over 3 cm from the beam axis is negligible.

Results for three experimental conditions are presented. During data run 1, $|\mathbf{B}_0|=30$ G, $\tau_b=3$ μs, $I_b\sim2.5$ A, grid positions $z_1=1$ cm, $z_2=44$ cm from the beam cathode face; initially, $n=2.2\times10^{11}$ cm^{-3}, $kT_e=0.6$ eV.

During data runs 2 and 3, $|\mathbf{B}_0| = 120$ G, $\tau_b = 5$ μs, grid positions $z_1 = 1$ cm, $z_2 = 25$ cm; initially, $n = 3.5 \times 10^{11}$ cm^{-3}, $kT_e = 0.3$ eV. I_b during data run 2 was 0.5 A; during data run 3, 1.5 A.

In each case, the beam drastically increases kT_e over a very short time (~ 1 μs) in the beam-flux tube, as shown for data run 3 in Fig. 2. Inside the beam-flux tube, n increases rapidly during the beam, because of ionization by the grid-confined tail electrons.[7] This creates a sharp density gradient (during data run 3, $|\nabla n/n|$ rose to 1/cm, at beam edge). Both ions and electrons drift outward from the beam flux tube, in response to the density gradient; during data run 3, electron radial velocities of $\sim 10^4$– 10^5 cm/s were found.

kT_e is roughly constant in the middle of the beam-flux tube, leading to difficulty in solving (4) there; $\kappa_\perp$ is not calculated near the edge of the system, or at late times in the data set, as small spatial and temporal derivatives yield inaccurate results.

Results for $\kappa_\perp$ in each of the three data runs are presented in Fig. 3. For the cases $|\mathbf{B}_0| = 30$ G and $I_b = 0.5$ A, $|\mathbf{B}_0| = 120$ G, $\kappa_\perp$ converges very nearly to predicted values (within a factor of 3) after beam turnoff. This is an experimental confirmation of classical transport theory.

During the beam pulse, for $|\mathbf{B}_0| = 120$ G, $\kappa_\perp$ exceeds classical expectations by over 2 orders of magnitude. Significantly higher values of $\kappa_\perp$ than predicted are also measured during the beam pulse for the case $|\mathbf{B}_0| = 30$ G, as well as after the beam pulse for the $I_b = 1.5$ A, $|\mathbf{B}_0| = 120$ G. This implies that other causes of heat flow, in addition to collisional, are present. It has been theoretically shown[8] that ion acoustic waves may be driven unstable by electron thermal gradients; this instability increases $\kappa_\perp$ to $\frac{13}{8}(\pi/2)^{1/2}|e\phi/kT_e|^2(\omega_{pe}/\omega_{ce}^2) \times (nkT_e/m)$ (approximating the ion acoustic spectrum by an average mode with $k = k_D/2$). Ion acoustic waves have been observed in electron-beam/plasma systems.[4] In one experiment,[4] without grids, $|\delta n/n| \sim |e\phi/kT_e| \sim 0.01$–$0.06$; for $n = 3 \times 10^{11}$ cm^{-3}, $kT_e = 2$

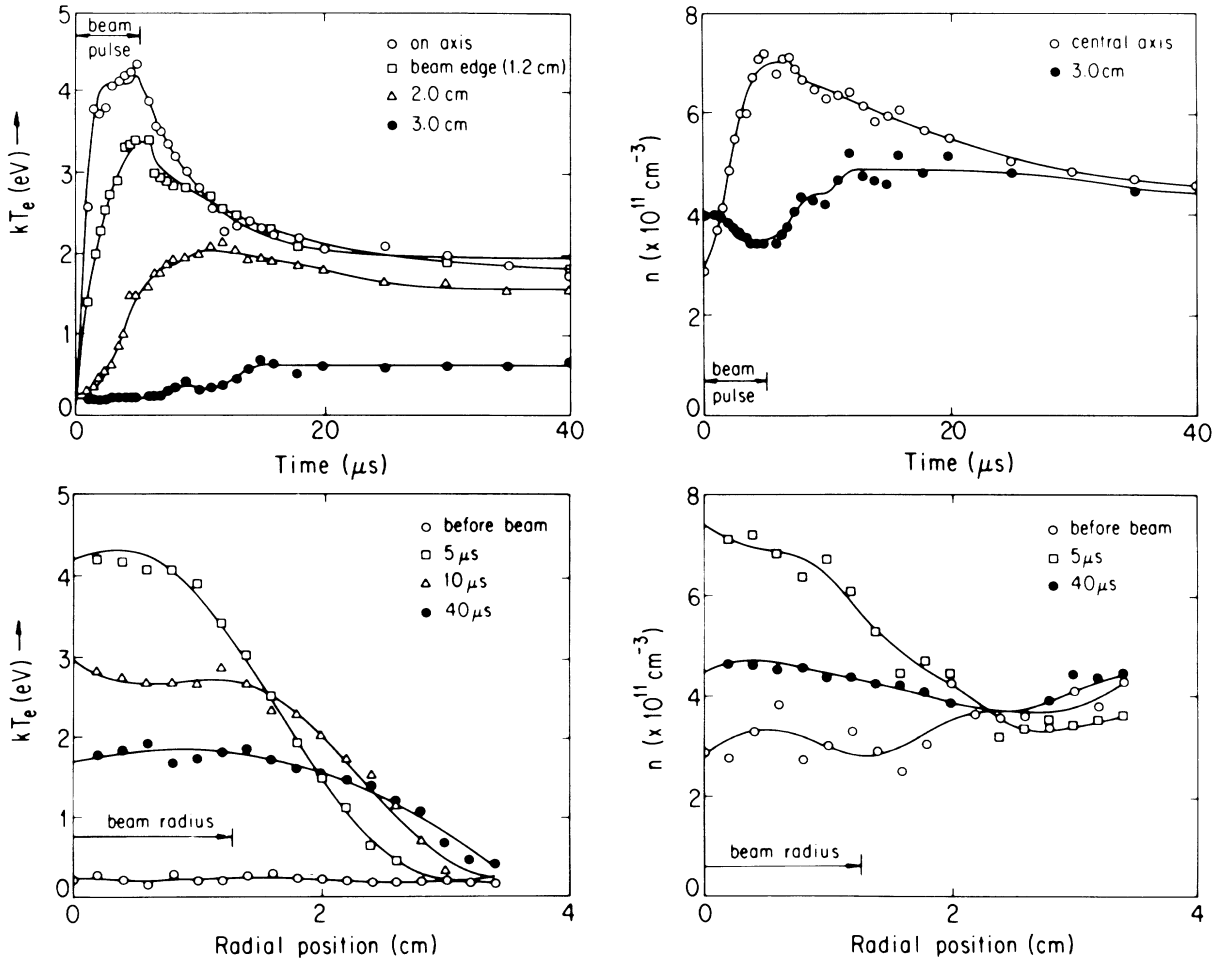

FIG. 2. kT_e and n vs radial position and time for $|\mathbf{B}_0| = 120$ G, $I_b = 1.5$ A. Symbols are experimentally measured points; solid lines are curve fits to the data, used for calculation of derivatives. Times are measured from beam turn-on; positions are measured from central axis.

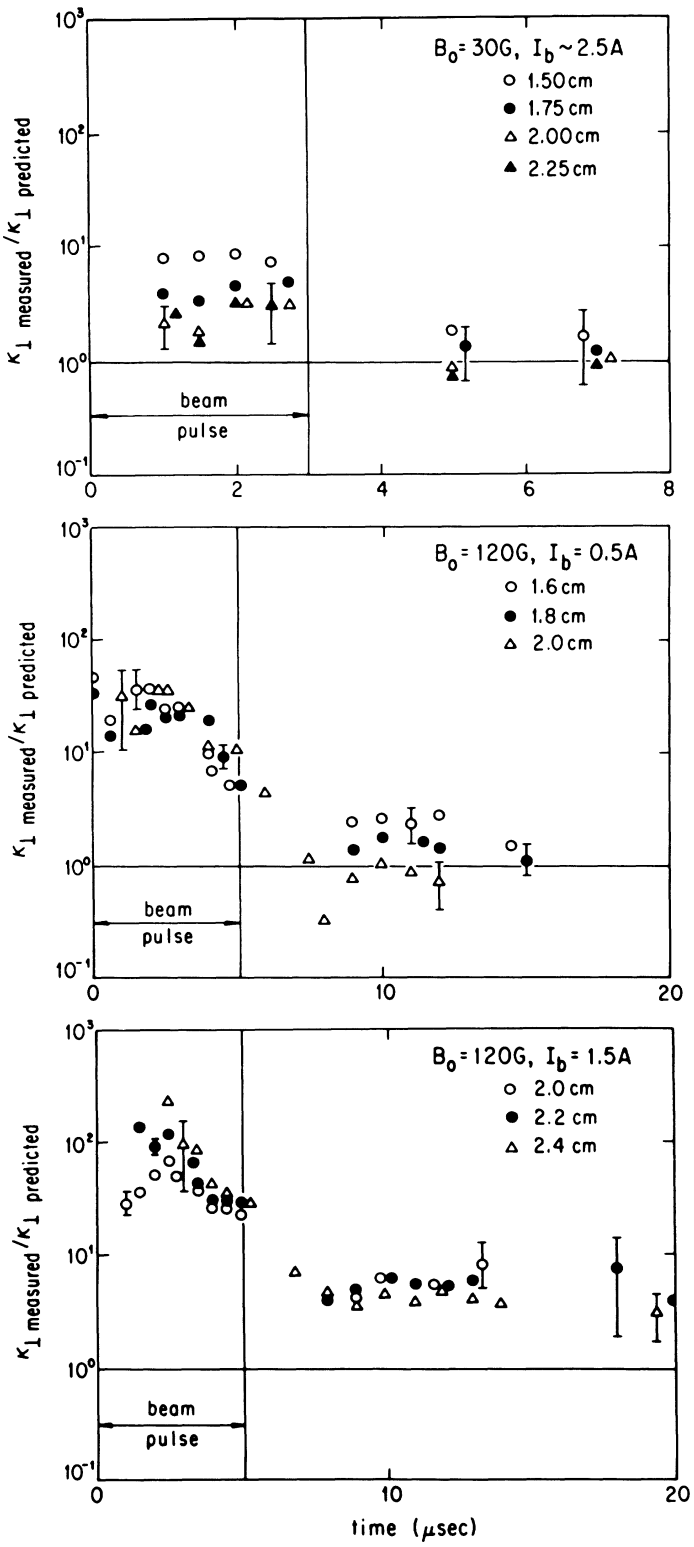

FIG. 3. $\kappa_\perp$ vs time for each of the three data runs. Error bars represent standard deviations. Times are measured from beam turnon; positions are measured from central axis.

eV, this increases the predicted $\kappa_\perp$ by a factor of up to 17. The waves are found to damp out ~ 2 μs after beam turnoff.[4] It is believed that an effect of the electrostatic trapping of the grids is to increase $\delta n/n$, and decay time of the waves, causing the anomalously high $\kappa_\perp$ values measured. For $|\mathbf{B}_0| = 120$ G, with pulsed grids, the authors detected significant wave activity ($f \sim 1$–15 MHz, $|e\phi/kT_e| \sim 0.10$) during the beam pulse ($I_b = 1.5$ A), as well as activity ($f \sim 1$ MHz, $|e\phi/kT_e| \sim 0.05$) for ~ 10 μs after beam turnoff. The dispersion relation of these waves is being investigated; it seems likely that these waves are azimuthal ion acoustic waves responsible for the high measurements of $\kappa_\perp$ during the 120-G measurements.

More accurate evaluation of $\kappa_{\perp\,\text{measured}}/\kappa_{\perp\,\text{predicted}}$ is not feasible with the present experimental setup. Estimated measurement errors in kT_e and n are $\sim 5\%$ and $\sim 10\%$, respectively. As $\kappa_{\perp\,\text{predicted}} \propto n^2/(kT_e)^{1/2}$, the uncertainty in $\kappa_{\perp\,\text{predicted}}$ is $\sim 22\%$. Much larger errors result from calculation of $\kappa_{\perp\,\text{measured}}$, due primarily to the multiple evaluations of partial derivatives. Errors are determined by use of a pseudorandom number generator to alter the various measurements of κT_e and n, within the measurement errors, then reevaluating (4) based on the new values. This procedure is repeated m times. By use of the m values, an average and standard deviation of $\kappa_{\perp\,\text{measured}}/\kappa_{\perp\,\text{predicted}}$ is calculated for each r and t. m is determined empirically. The standard deviations are indicated by error bars in Fig. 3.

We wish to thank Mr. L.-Y. Chan, Mr. J. M. Urrutia, and Dr. W. Gekelman for many useful discussions. This research is supported by National Science Foundation Grants No. PHY-84-10495 and No. ATM-84-01322 and University of California Academic Research Grant No. UCLA-ASRC-3673.

[1]R. Landshoff, Phys. Rev. **76**, 904 (1949).

[2]F. Rostas, A. K. Bhattacharya, and J. H. Cahn, Phys. Rev. **129**, 495 (1963).

[3]S. I. Braginskii, Zh. Eksp. Teor. Fiz. **33**, 459 (1958) [Sov. Phys. JETP **6**, 358 (1958)].

[4]D. A. Whelan and R. L. Stenzel, Phys. Fluids **28**, 958 (1985).

[5]S. I. Braginskii, *Transport Processes in a Plasma,* Reviews of Plasma Physics Vol. 1 (Consultants Bureau, New York, 1965), p. 205.

[6]L.-Y. Chan, private communication.

[7]K. Papadopoulos, in *Artificial Particle Beams in Space Plasma Studies,* edited by Bjørn Grandal, NATO Advanced Study Institute Series B: Physics Vol. 79 (Plenum, New York, 1982), p. 505.

[8]W. M. Manheimer, C. E. Max, and J. Thomson, Phys. Fluids **21**, 2009 (1978).